Chemical Engineering Journal 294 (2016) 97–104

Contents lists available at ScienceDirect

Chemical Engineering Journal

journal homepage: www.elsevier.com/locate/cej

Coupling exothermic and endothermic reactions in an ethanol microreformer for H_2 production

Yanina M. Bruschi *, Eduardo López, Marisa N. Pedernera, Daniel O. Borio

PLAPIQUI (UNS-CONICET), Camino La Carrindanga, km. 7, 8000 Bahía Blanca, Argentina

HIGHLIGHTS

- A micro-reformer is simulated to study the ethanol steam reforming (ESR) reaction.
- The ESR reaction is thermally coupled with the ethanol combustion.
- To reach high production rates, an adequate preheating of both streams is necessary.
- Hydrogen yields relatively high are obtained within a feasible range of temperatures.

ARTICLE INFO

Article history:
Received 12 November 2015
Received in revised form 10 February 2016
Accepted 19 February 2016
Available online 3 March 2016

Keywords:
Ethanol steam reforming
Thermal coupling
Ethanol combustion
Microreactor

ABSTRACT

The steam reforming of ethanol is carried out in a microreactor for hydrogen production. The heat for the endothermic reactions is supplied by means of ethanol combustion in air, which is carried out in contiguous microchannels. The same Pd-based catalyst is assumed to be coated on both reforming and combustion channels. By means of a 1D heterogeneous mathematical model, the influence of the feed temperatures of both streams on the reactor performance is analyzed. The results show that the degree of preheating of both streams has a strong influence on the hydrogen yields and maximum temperatures. The effect of the flowrate and composition of the fuel stream on the hydrogen yields is also studied.

Fairly high hydrogen yields were obtained ($2.6 < \eta_{H_2} < 3.4$) with low methane slips, within a feasible range of temperatures for the Pd catalyst ($700 < T_{MAX} < 770$ °C) to avoid catalyst deactivation. These maximum temperatures could still be further reduced by means of an optimal selection of the air flowrate and ethanol molar fraction on the fuel side, or using distributed feed of fuel along the reactor length.

1. Introduction

Fuel cells using hydrogen require an efficient and flexible hydrogen supply [1]. Therefore, it is important to develop efficient stand-alone processes for the production of pure hydrogen. Bioethanol is an attractive raw material for the production of hydrogen or syngas, because of its renewability, high energy density and low toxicity and volatility. In the last years, some attention has been paid to processes for the production of H_2 or synthesis gas from ethanol by means of catalytic steam reforming (*ESR*) [2–4]. Since the reactions are highly endothermic, reactors with efficient heat transfer to the process side are required.

Microreactors provide a high surface to volume ratio and high heat and mass transfer coefficients, which makes them appropriate for processes requiring high heat-fluxes per unit area, as in catalytic steam reforming of hydrocarbons or alcohols [5]. By means of a 3D CFD model, Uriz et al. [6] have demonstrated the strong influence of the microchannel size on the performance of a microreactor for ESR.

Because of the small geometry and the high heat conductivity of the materials, lab-scale microreactors can be electrically heated and isothermal conditions can usually be assumed [7]. However, under higher production-scale conditions, the heat supply for the steam reforming should be provided through other sources, e.g., convective heating using flue gas coming from an external combustion chamber [8,9], simultaneous steam reforming and partial oxidation in the same channel, named autothermal reforming (ATR) [10–13], or thermal coupling of steam reforming and oxidation reactions in contiguous channels [14].

Different studies for the coupling of exothermic and endothermic reactions have been published [15–16]. Frauhammer et al. [17] and Kolios et al. [18] have analyzed the methane steam reforming coupled with methane combustion; their results

* Corresponding author.
E-mail address: ybruschi@plapiqui.edu.ar (Y.M. Bruschi).

http://dx.doi.org/10.1016/j.cej.2016.02.079
1385-8947/

Nomenclature

a	heat transfer area per unit volume $2bL/(b^2L)$, m^2/m^3
a'	mas transfer area per unit volume $3bL/(b^2L)$, m^2/m^3
A_T	cross sectional area of channels b^2, m^2
b	width of square channel, m
C_p	specific heat, J/(mol K)
C	molar concentration, mol/m^3
CHR	consumed heat rate, kW/m
d_h	hydraulic diameter b, m
D_m	molecular diffusivity (m^2/s)
Ea_i	Activation energy of reaction i (process side), $i = r1, r2, r3$, kJ/mol
Ea_i^C	Activation energy of reaction i (combustion side), $i = r4, r5$, kJ/mol
e	fin width, μm
F	molar flow, mol/s
h	heat transfer coefficient, $W/(m^2\ K)$
ΔH_i	heat of reaction i (process side), $i = r1, r2, r3$, J/mol
ΔH_i^C	heat of reaction i (combustion side), $i = r4, r5$, J/mol
$k_{\infty\ i}$	pre-exponential factor of reaction i (process side), $i = r1, r2, r3$, $kmol/(m^3\ s\ bar^n)$
$k_{i,\ ref}^C$	pre-exponential factor of reaction i (combustion side), $i = r4, r5$, $mol/(m^2\ s\ bar)$
k_i	reaction rate constant (process side), $i = r1, r2, r3$, $kmol/(m^3\ s\ bar^n)$
k_i^C	reaction rate constant (combustion side), $i = r4, r5$, $mol/(m^2\ s\ bar)$
k_g	mass transfer coefficient, (m/s)
$K_{eq\ i}$	equilibrium constant for reaction i, $i = r2, r3$
L	channel length, m
NC	number of microchannels
Nu	Nusselt number hd_h/λ, dimensionless
P	total pressure (both sides), MPa
p	partial pressure, bar
Pr	Prandlt number $C_P\mu/\lambda$, dimenssionless
r_i	reaction rate of reaction i (process side), $i = r1, r2, r3$, $mol/(m^3\ s)$
r_i^C	reaction rate of reaction i (combustion side), $i = r4, r5$, $mol/(m^2\ s)$
Re	Reynolds number $\rho u d_h/\mu$, dimensionless
RHR	released heat rate, kW/m
Sc	Schmidt number $\mu/\rho D_m$, dimensionless
Sh	Sherwood number $k_g d_h/D_m$, dimensionless
S/C	Steam to carbon molar ratio, mol H_2O/mol C
T	temperature, °C
$T_{ref\ 4}^C$	reference temperature of reaction $r4$, °C
$T_{ref\ 5}^C$	reference temperature of reaction $r5$, °C
u	average velocity, m/s
wc	thickness of the washcoated catalyst, μm
y	molar fraction, dimensionless
z	axial coordinate, m

Greek letters

ρ	density, kg/m^3
μ	viscosity, Pa s
η	yield, dimensionless
λ	thermal conductivity, W/(m K)
ν	stoichiometric coefficient

Subscripts

Ac	acetaldehyde
CO	carbon dioxide
CO_2	carbon monoxide
CH_4	methane
Et	ethanol
H_2	hydrogen
H_2O	water
MAX	maximum value
N_2	nitrogen
O_2	oxygen
j	component j
k	component k
i	reaction i
S	solid phase
0	at the axial coordinate $z = 0$
L	at the axial coordinate $z = L$

Superscripts

C	Combustion side

revealed that the heat released in the combustion reaction can be transferred efficiently to the process side. However, excessive temperatures can arise inside the reactor due to the fast and strongly exothermic oxidation reactions. Kolios et al. [19] studied different strategies for thermal coupling between endothermic (steam reforming of methane and methanol) and different exothermic reactions, including distributed feed of the fuel. Particularly, López et al. [20] have studied a thermally coupled reactor for ethanol steam reforming. The necessary heat for this endothermic reaction was provided by hydrogen combustion. An experimental study of the ESR process was published by Casanovas et al. [14]. A microreactor was used to study the thermal coupling of reactions with different catalysts coated on the reactor walls for each side. The same reactant (ethanol) was employed on the endothermic and exothermic channels [14].

In the present work, the performance of a microreactor for hydrogen generation by ESR is studied. Among the different strategies to provide the heat for the reforming reactions, thermal coupling between ESR and ethanol combustion in contiguous channels has been adopted. To carry out the simulations, the same Pd-based catalyst is assumed for all the channels and a co-current configuration between the process and fuel streams is adopted. The feasibility of the proposed design to produce hydrogen efficiently is analyzed. A possible range for the operating conditions is explored, leading to reach high hydrogen yields without exceeding the maximum allowable temperatures.

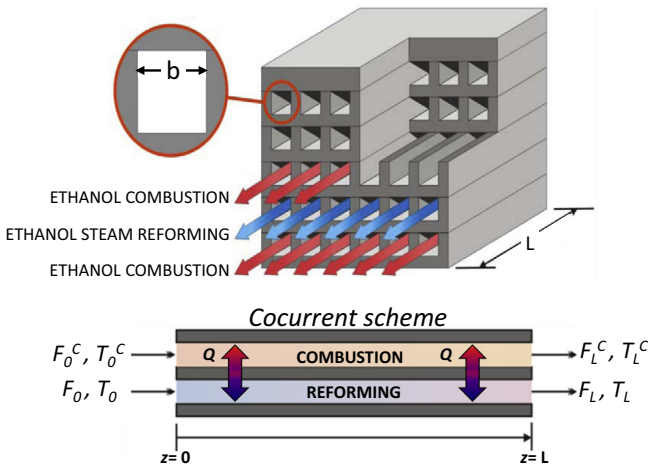

Fig. 1. Scheme of the simulated reformer.

2. Mathematical model

A steady-state 1-D heterogeneous model is selected to simulate the microreactor represented in Fig. 1 [8]. As shown, adjacent foils are used to circulate co-currently the process mixture (ethanol + H_2O) and the fuel stream (ethanol + air), which supplies the heat required for the endothermic reforming reactions.

The reactions set considered in the ESR process and the ethanol catalytic combustion are detailed in Table 1. Reaction ($r1$) is assumed as irreversible, whereas reactions ($r2$) and ($r3$) are equilibrium-limited [20]. Reaction ($r4$) represents the ethanol partial oxidation and reaction ($r5$) the acetaldehyde combustion [21]. Both kinetic models are effective, i.e., the reaction rate expressions include the mass-transfer limitations inside the washcoat. The rate expressions for all the reactions considered in this work are presented in Eqs. (1)–(5).

2.1. Reforming side

$$r_1 = k_1 p_{Et} p_{H_2O} \tag{1}$$

$$r_2 = k_2 p_{CH_4} p_{H_2O} \left(1 - \frac{1}{K_{eq2}} \frac{p_{CO} p_{H_2}^3}{p_{CH_4} p_{H_2O}}\right) \tag{2}$$

$$r_3 = k_3 p_{CO} p_{H_2O} \left(1 - \frac{1}{K_{eq3}} \frac{p_{CO_2} p_{H_2}}{p_{CO} p_{H_2O}}\right) \tag{3}$$

where the equilibrium constants appearing in Eqs. (2) and (3) were calculated by standard thermodynamic relations for real gases [22]. The values for the kinetic parameters were estimated by Lopez et al. [20] and are presented in Table 2.

2.2. Combustion side

$$r_4^C = k_4^C p_{Et,S}^C \tag{4}$$

$$r_5^C = k_5^C p_{Ac,S}^C \tag{5}$$

The values for the kinetic parameters estimated by Bruschi [21] are shown in Table 3.

The mathematical model is based on the same assumptions than those by Bruschi et al. [9]:

Table 1
Scheme of reactions.

Reforming side	
($r1$) $C_2H_5OH + H_2O \rightarrow CH_4 + CO_2 + 2H_2$	ΔH_1 = 8.73 kJ/mol
($r2$) $CH_4 + H_2O \leftrightarrow CO + 3H_2$	ΔH_2 = 205.8 kJ/mol
($r3$) $CO + H_2O \leftrightarrow CO_2 + H_2$	ΔH_3 = −41.17 kJ/mol
Combustion side	
($r4$) $C_2H_5OH + 1/2\ O_2 \rightarrow CH_3CHO + H_2O$	ΔH_{4c} = −172.9 kJ/mol
($r5$) $CH_3CHO + 5/2\ O_2 \rightarrow 2\ CO_2 + 2\ H_2O$	ΔH_{5c} = −1104.5 kJ/mol

Table 2
Reaction rate parameters for Eqs. (1)–(3) (Reforming side) [20]. $k_i = k_{\infty,i} e^{-Ea/RT}$.

i	$k_{\infty,i}$ [kmol/m^3/seg/bar^n]	Ea_i [kJ/mol]
1	2.4×10^9	148
2	2.1×10^6	107.3
3	7.7×10^2	59.9

Table 3
Reaction rate parameters for Eqs. (4) and (5) (Combustion side) [21]. $k_i^C = k_{i,ref}^C e^{-\frac{Ea}{R}\left(\frac{1}{T^C} - \frac{1}{T_{ref,i}^C}\right)}$, $T_{ref,4}^C$ = 598 K and $T_{ref,5}^C$ = 723 K.

i	$k_{i,ref}^C$ [mol/m^2/seg/bar]	Ea_i^C [kJ/mol]
4	0.661	169.1
5	1.233	135.9

(a) Isobaric conditions: the laminar flow through short channels without pellets ensures low pressure drop.
(b) Heat losses from the microreactor to the environment are neglected (the reactor is assumed to be properly isolated).
(c) Axial dispersion phenomena are neglected, considering laminar flow for both process and combustion fluids.
(d) Temperature and composition gradients are neglected in a cross section of a channel due to the small dimensions at hand.
(e) Uniform flow distribution among all the microchannels (a proper flow distributor is assumed [23,24].
(f) Two contiguous channels (process and combustion sides) are modeled as representative of the whole microreactor.
(g) Two additional assumptions are assumed in the present contribution:
(h) The heat-transfer resistances in the gas–solid interface are taken into account on both the reforming and combustion sides. In the combustion channels, the external mass-transfer limitations are considered as well.
(i) A single temperature value is assumed in the solid phase (metal wall and catalyst) for every axial position and for both sides (reforming and combustion).

From these assumptions, the mathematical model is constituted by the equations presented in Table 4. The symbols F_j y F_k^C note the molar flows of species j and k per channel, flowing on the reactants and combustion sides, respectively.

The thermodynamic properties of the components are taken from literature [22,25]. The heat transfer convective coefficients for each side (h and h_C) and the mass transfer coefficients ($k_{g,k}$) are obtained from the *Nusselt* and *Sherwood* expresions proposed by Cybulski et al. [26] for square-channels structured reactors:

$$Nu = \frac{h d_h}{\lambda} = 2.978 \left(1 + 0.095\,\mathrm{Re}\,\mathrm{Pr}\,\frac{b}{L}\right)^{0.45} \tag{12}$$

$$Sh_k = \frac{k_{g,k} d_h}{D_{m,k}} = 2.978 \left(1 + 0.095\,\mathrm{Re}\,Sc_k\,\frac{b}{L}\right)^{0.45} \tag{13}$$

Eqs. (6)–(11) constitute a differential–algebraic problem. This DAE system was integrated by a specific solver (*DASolver*) with the *Process Systems Enterprise gPROMS* program.

The geometric parameters considered in the simulations are given in Table 5. The reference size of the microchannels (b = 200 μm) is based on that proposed by Görke et al. [7]. A total number of 31600 channels (158 foils of 200 channels) are selected for both, the reforming and combustion sides. The same Pd-based catalyst is assumed to be coated on the metallic microchannels for both the process and combustion sides. As in the previous contribution by López et al. [20], a washcoat thickness of wc = 10 μm was adopted.

3. Results and discussion

The results presented in this paper were obtained changing the operating conditions for the same channel geometry. The operating

Table 4
Mathematical model.

	Reforming side	Combustion side
Gas phase	*Mass balance:* $\frac{dF_j}{dz} = A_T \sum_i (v_{j,i} r_i)$ (6) B.C.: at $z = 0$; $F_j = F_{j,0}$ for j = *Et*, H_2O, CH_4, CO_2, CO, H_2 i = 1, 2, 3 (Reactions for process side, Table 1)	*Mass balance:* $-\frac{dF_k^C}{dz} = A_T a' k_{g,k} \left(C_k^C - C_{k,S}^C\right)$ (8) B.C.: at $z = 0$; $F_k = F_{k,0}$ for k = *Et*, O_2, H_2O, CO_2, Ac, N_2
	Energy balance: $F Cp \frac{dT}{dz} = A_T h a (T_S - T)$ (7) B.C.: at $z = 0$; $T = T_0$	*Energy balance:* $F^C Cp^C \frac{dT^C}{dz} = A_T h^C a (T_S - T^C)$ (9) B.C.: *at* $z = 0$; $T^C = T^C{}_0$
Solid phase		*Mass balance:* $k_{g,k} \left(C_k^C - C_{k,S}^C\right) + \sum_i (v_{k,i} r_i^C) = 0$ (10) for k = Et, O_2, H_2O, CO_2, Ac, N_2 i = 4, 5 (Reactions for combustion side, Table 1)
	Energy balance: $-a' A_T \left(r_4^C \Delta H_4^C + r_5^C \Delta H_5^C\right) - A_T (r_1 \Delta H_1 + r_2 \Delta H_2 + r_3 \Delta H_3) + h^C a' A_T (T^C - T_S) + h a A_T (T - T_S) = 0$ (11) A single energy balance for the soild phase is proposed, int the line with the hypothesis (h).	

Table 5
Geometric parameters.

Channel length, L*	0.08 m
Channel width = height, b*	200 μm
Fin width, e*	100 μm
Channels per foil	200
Number of channels (each side), NC	31600
Height of stack	9.48 cm
Thickness of the washcoated catalyst, wc*	10 μm
Coated surface of stack	1.51 m^2

* Görke et al. [7].

Table 6
Operating conditions adopted in the simulations.

Reforming side	
Pressure, P	0.1 MPa
Inlet temperature, T_0	100–800 °C
Feed molar flowrate, F_0	0.13 mol/s
Steam to carbon ratio, S/C	3
Combustion side:	
Pressure, P	0.1 MPa
Inlet temperature, T_0^C	100–600 °C
Feed molar Flowrate, F_0^C	0.18 mol/s
Ethanol molar fraction, $y_{Et,0}^C$	0.01–0.03

conditions used are presented in Table 6. A typical feed composition for ethanol steam reforming is assumed, i.e., *S/C* = 3 [27]. The flow of ethanol fed to the microreactor on the process side is selected so that a hydrogen-rich stream of 10 kWth equivalent can be achieved. A similar total molar flowrate is adopted for the fuel side.

3.1. Coupling ethanol reforming and ethanol combustion under cocurrent flow

To introduce to the analysis of the ethanol reformer under cocurrent flow, it has been selected an operating condition where the feed temperature on the combustion side is lower than the feed temperature on the reforming side, i.e., T_0^C = 100 °C; T_0 = 540 °C. Fig. 2c shows the axial temperature profiles for the solid phase (T_S), reforming gas phase (T) and combustion gas phase (T^C). Due to the high values of the heat transfer area and heat transfer coefficients, the reforming stream preheats rapidly the fuel gas until the temperatures approximate one another at a value of around 340 °C (see the zoom in Fig. 2c). In this zone, the temperature is still too low to let the reforming reactions take place (see Fig. 2b), but high enough to start the reactions on the combustion side. As shown in Fig. 2a, the molar fraction of the fuel decreases from the reactor inlet as the acetaldehyde level increases, due to the ethanol partial oxidation (reaction (*r*4) of Table 2). This reaction is hardly exothermic, and consequently the temperature rise in this reactor zone is moderate. Once the acetaldehyde level and the solid temperature are high enough to ignite the highly exothermic reaction (*r*5) ($\Delta H_5 = -1104.5$ kJ/mol), the temperature profiles show a steep increase up to 680 °C. This strong temperature rise is associated to a fast increase in the molar fraction of CO_2 (Fig. 2a). The temperature rise lets the reforming reactions start, and an initial increase in the molar fractions of H_2, CH_4 and CO_2 is observed, mainly as a consequence of reaction (*r*1) (ethanol decomposition). Downstream the temperature peak, additional amounts of H_2 are generated due to methane reforming and water gas shift (reactions (*r*2) and (*r*3)). Nevertheless, the outlet hydrogen yield for this operating condition is relatively low ($\eta_{H_2} = 2.4$)), as a consequence of the residual amounts of CH_4. Beyond z = 3 cm the temperatures show a continuous decrease, as a result of the occurrence of the strongly endothermic reaction (*r*2) and the reaction depletion on the combustion side. To complete the analysis, Fig. 2d shows the axial profiles of the released heat rate on the combustion side (*RHR*, Eq. (14)) and the consumed heat rate on the reforming side (*CHR*, Eq. (15)).

$$RHR = \left| NC\,3\,B \sum_1^2 r_i^C \Delta H_i^C \right| \tag{14}$$

$$CHR = NC\,B^2 \sum_1^3 r_i \Delta H_i \tag{15}$$

It is important to note that the rates of the oxidation reactions (*r*4) and (*r*5) are notably higher than those of the reforming reactions (*r*1) to (*r*3). As a result, the combustion heat is released in a narrow zone of the reactor and the *RHR* reaches extremely high values (note the different scales on both ordinate axis of Fig. 2d). On the other side of the process, the ethanol reforming takes place in a more extensive region downstream the location of the peak in *RHR*. Analogous phenomena have been reported by Kolios et al. [19] for the case of reactions coupling in a methane steam reformer. A distributed feed of fuel was proposed to attenuate the temperature peaks and improve the reactor performance. The

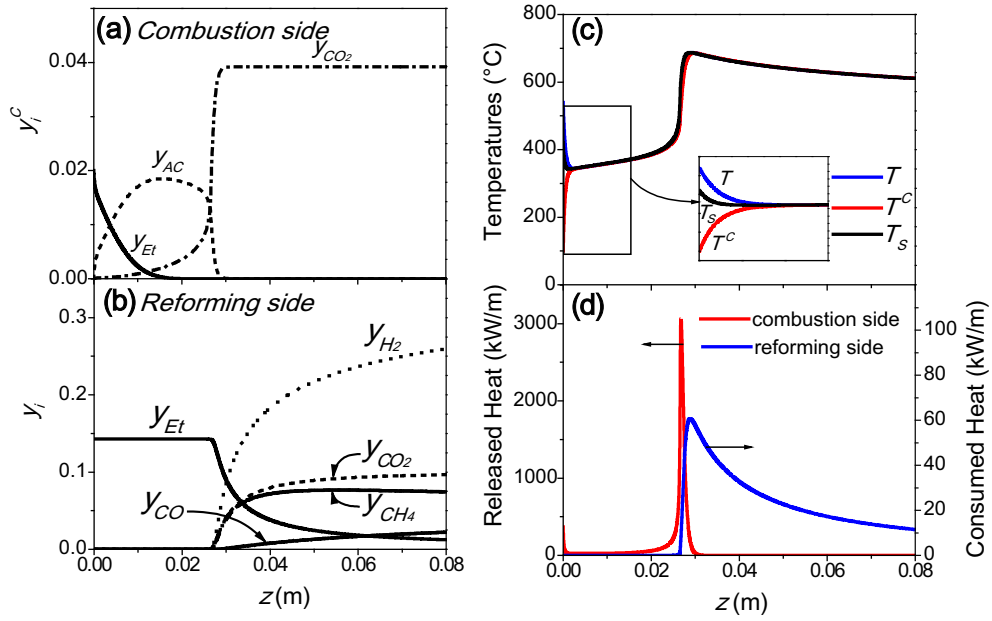

Fig. 2. Axial profiles for a particular operating condition: T_0 = 540 °C, T_0^C = 100 °C, $y_{Et,0}^C$ = 0.02 and F_0^C = 0.18 mol/s. (a) Molar fraction of different compounds on the combustion side. (b) Molar fraction of different compounds on the reforming side. (c) Temperature profiles for both streams and for the solid phase. (d) The heat released by the exothermic reactions and the heat consumed by the endothermic reactions.

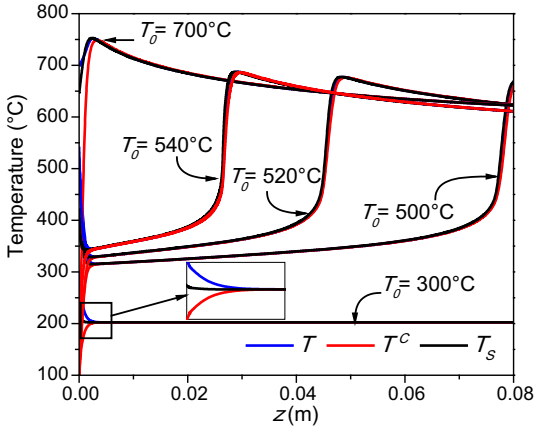

Fig. 3. Temperature axial profiles for a constant value of combustion inlet temperature (T_0^C = 100 °C) and different T_0 values. $y_{Et,0}^C$ = 0.02 and F_0^C = 0.18 mol/s.

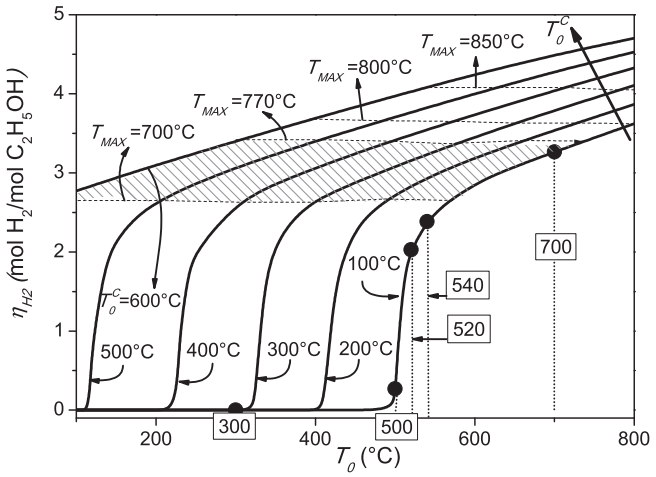

Fig. 4. Hydrogen yield as affected by the reforming inlet temperature (T_0) for different combustion inlet temperatures (T_0^C). $y_{Et,0}^C$ = 0.02 and F_0^C = 0.18 mol/s.

substantial difference between the rates of the exothermic and endothermic reactions is the main challenge for a proper design of the reformer, when reaction coupling is employed.

3.2. Influence of the inlet temperatures: ignition curves

Fig. 3 shows axial temperature profiles for a constant feed temperature on the combustion side (T_0^C = 100 °C) and different feed temperatures for the reforming side (T_0). In the case of T_0 = 300 °C, the inlet temperatures of both streams are too low to reach the ignition temperature on the combustion side; consequently, the reactions are practically extinguished and the temperature profiles become constant at around 200 °C. For T_0 = 500 °C, a sudden temperature rise close to the reactor outlet is observed, in a similar way as described in Fig. 2c. If higher values of T_0 are selected, the ignition phenomenon shifts rapidly to the left and for the particular case T_0 = 700 °C the hot spot is located near the reactor entrance. Under these conditions, the hydrogen yield is relatively high (around 3.3) and the hot spot value is T_{MAX} = 755 °C. This maximum temperature is still below the highest temperature at which the Pd catalyst was tested by López et al. [20] at laboratory conditions (T_{MAX} = 770 °C), without any apparent catalyst deactivation.

Fig. 4 shows the outlet hydrogen yields (η_{H_2}) for a wide range of inlet temperatures on both sides of the process. The remaining operating conditions are kept constant at the values detailed in Table 4, for a particular ethanol molar fraction on the combustion side, i.e., $y_{Et,0}^C$ = 0.02. Each curve corresponds to a constant feed temperature on the combustion side ($T_{C,0}$), showing three main zones. The first zone is located to the left of the ignition point, where the reactions are extinguished and η_{H_2} is zero. Once the advance of the combustion reactions is significant, the yield shows a sudden improvement within a narrow range of T_0 values. In the third zone, for higher feed temperatures on the reforming side, the reactor is completely ignited and the hydrogen yield increases more gradually. The circles

marked on the lower curve of Fig. 4 (for T_0^C = 100 °C) correspond to the outlet hydrogen yields of the five operating conditions presented in Fig. 3. Finally, Fig. 4 shows clearly that the ignition phenomenon occurs at lower T_0 values as $T_{C,0}$ is increased; e.g., if the fuel stream is preheated up to 200 °C, the ignition occurs for T_0 = 400 °C; if the preheating is extended up T_0^C = 500 °C, the ignition takes place practically for T_0 = 120 °C, i.e., a process feed stream hardly above its boiling point. For T_0^C = 600 °C, the reactor would be ignited for the whole range of T_0 values. However, for high values of T_0^C another phenomenon can occur: the auto-ignition of the ethanol/air mixture before entering the reactor (the possible occurrence of homogeneous ethanol combustion has not been considered in the present work). Fig. 4 also includes curves joining points with the same maximum temperature, within the range 700–850 °C where the reactor is completely ignited. For these operating conditions, the curves of constant T_{MAX} are almost horizontal, i.e., each value of hydrogen yield is related approximately to a single value of T_{MAX}. It is clear that, for these operating conditions, reaching hydrogen values above $\eta_{H_2} = 4$ would require to operate the reactor at maximum temperatures higher than 800 °C. This high temperature values could be a challenge for avoiding catalyst deactivation. Nevertheless, within the shaded area in Fig. 4, hydrogen yields reasonable good (between 2.6 and 3.4) could be attained within a feasible temperature range for this Pd catalyst (T_{MAX} = 700–770 °C) [20].

Fig. 5 shows the outlet methane yields for the same conditions of Fig. 4. For each value of T_0^C, the curves present a sudden increase as a consequence of the ethanol decomposition reaction ($r1$), which is irreversible and quite fast. After the ignition point is reached, all the curves show maxima for a methane yield of around 0.7. Once the ethanol conversion is almost complete, the methane yield shows a continuous decrease due to a higher extension of the reversible and slower reaction ($r2$) (steam reforming of methane), which is the responsible of the gradual increase in η_{H_2} described in Fig. 4.

3.3. Influence of the inlet ethanol fraction (combustion side) on the reactor performance

The inlet ethanol fraction on the combustion side ($y_{Et,0}^C$) is directly related to the heat supply and consequently with the reactor performance. Fig. 6 shows the influence of this operating variable on the outlet hydrogen yield (Fig. 6a) and the maximum temperature reached inside the reactor (T_{MAX}, Fig. 6b). Each curve of Fig. 6 corresponds to a different feed temperature, but for all the cases $T_0 = T_0^C$. As expected, the hydrogen yield improves as the ethanol fuel increases, which is accompanied by higher values

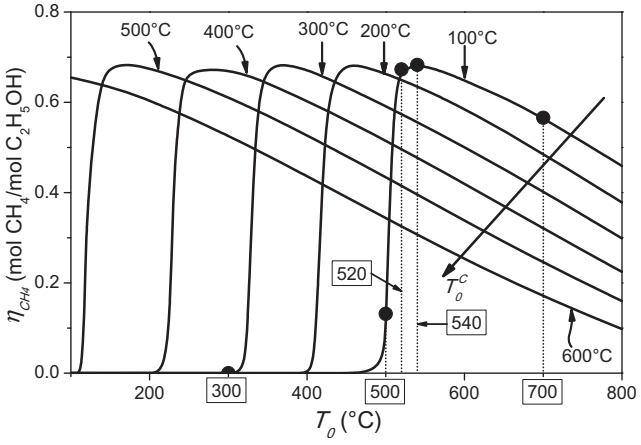

Fig. 5. Methane yield as affected by the reforming inlet temperature (T_0) for different combustion inlet temperatures (T_0^C). $y_{Et,0}^C$ = 0.02 and F_0^C = 0.18 mol/s.

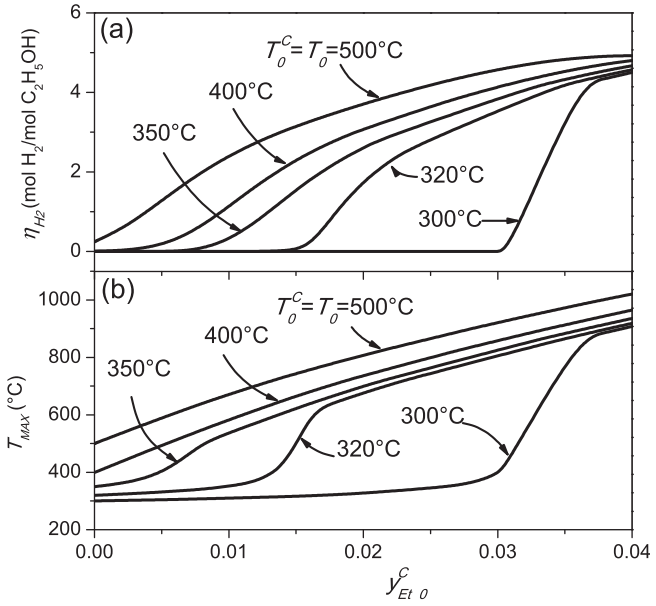

Fig. 6. The outlet hydrogen yield and the maximum temperature value reached inside the reactor as affected by the inlet ethanol fraction on the combustion side ($y_{Et,0}^C$) for different pairs of T_0^C and T_0. F_0^C = 0.18 mol/s.

of T_{MAX}. To reach a desired hydrogen production rate (i.e., a given value of η_{H_2}) higher amounts of ethanol fuel are necessary as lower feed temperatures are chosen. However, the behavior of the curves is strongly affected by the temperature level of the feed streams, which depends on the preheating strategy adopted to operate the reformer. When the feed temperatures are high enough (e.g., $T_0 = T_0^C$ = 500 °C), the enthalpies of both inlet streams let the reforming reactions to proceed ($\eta_{H_2} > 0$) even though the ethanol fed on the fuel side is zero. As $y_{Et,0}^C$ is augmented, more heat is released on the combustion side and consequently η_{H_2} and T_{MAX} exhibit a gradual increase. Conversely, when the preheating of both streams is not enough, curves of η_{H_2} and T_{MAX} are flat within a range of low values of $y_{Et,0}^C$ In the case of $T_0 = T_0^C$ = 320 °C, the ethanol molar fraction must be at least 1.4% to ignite the reactions on the combustion side. In fact, for $y_{Et,0}^C$ = 1.5%, the maximum temperature shows a sudden increase and the reformer begins to produce hydrogen. This behavior appears amplified for the case of $T_0 = T_0^C$ = 300 °C, occurring for $y_{Et,0}^C \approx 3\%$. To the right of the ignition phenomena, the curves present a gradual behavior, similar to that of T_0 = 500 °C.

Fig. 7 show the composition (molar fractions) of the flue-gas leaving the combustion side of the ethanol reformer, for some particular conditions shown in Fig. 6. For the case $T_0 = T_0^C$ = 500 °C, the ethanol combustion is almost complete for all the range of $y_{Et,0}^C$, only CO_2 appears at the reactor outlet and a straight line with slope 2 (stoiquiometric coefficient for CO_2) is observed. For the lower feed temperatures (300 and 320 °C), acetaldehyde appears for low values of $y_{Et,0}^C$ as a result of incomplete ethanol combustion (also low amounts of unconverted ethanol, not shown in Fig. 7). Under these conditions, the reformer would be emitting contaminants through the flue-gas. Once the temperature level is high enough to ignite reaction ($r5$), the intermediate acetaldehyde begins to decrease and a rapid rise in the CO_2 molar fraction occurs.

3.4. Effect of the fuel stream: ethanol molar fraction vs. total flowrate

The heat generation rate on the combustion side depends on the amount of ethanol fuel ($F_{Et,0}^C$) fed to the reformer. The effect of $F_{Et,0}^C$

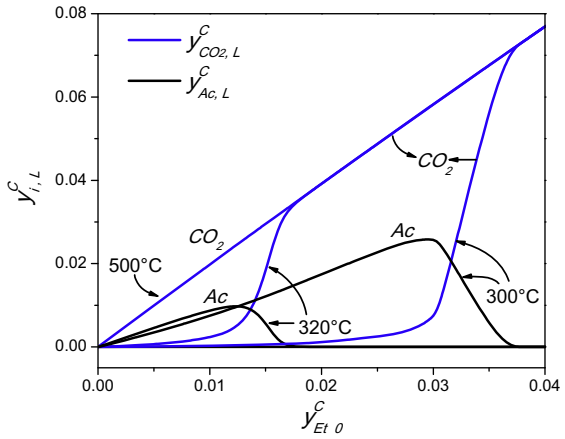

Fig. 7. The outlet Acetaldehyde and CO_2 molar fraction on the combustion side as affected by the inlet ethanol fraction ($y^C_{Et,0}$) on the same stream for some temperatures of Fig. 6.

on the hydrogen production is shown in Fig. 8, for two different values of the feed temperature (320 and 500 °C).

The ethanol flowrate in the fuel stream (Eq. (16)) can be modified by means of two different policies.

$$F^C_{Et,0} = y^C_{Et,0}\, F^C_0 \tag{16}$$

One of them is varying the ethanol fraction ($y^C_{Et,0}$), keeping constant the total combustion flowrate (F^C_0), as it was analyzed in the previous section. This strategy is represented by curves in dashed lines in Fig. 8. Another policy is varying F^C_0, keeping constant the value of $y^C_{Et,0}$, which corresponds to the curves in solid lines of Fig. 8.

Both curves for $T_0 = T^C_0 = 500$ °C differ slightly from each other when the ethanol flowrate is varied. That is, if the preheating of the feed streams is adequate, the hydrogen production rate is determined by the ethanol fuel fed to the reformer, almost independently of the total flowrate used on the combustion side. On the other hand, when the feed stream are not preheated enough ($T_0 = T^C_0 = 320$ °C), the hydrogen production rate depends strongly on the selected value of F^C_0. When F^C_0 is kept constant at 0.18 mol/h and $y^C_{Et,0}$ is varied (curve in dashed line), as shown in

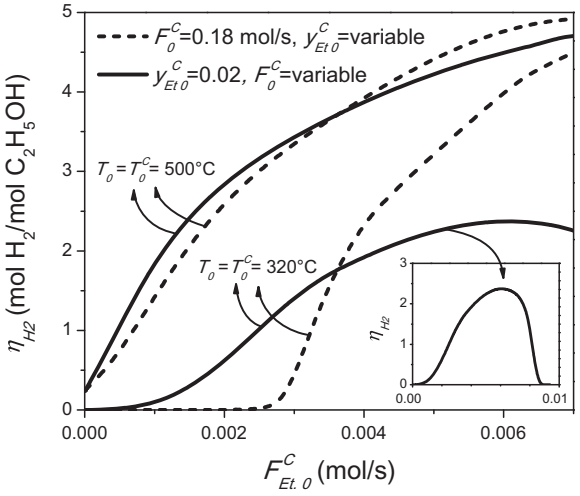

Fig. 8. Hydrogen yield as affected by the inlet ethanol flowrate on the combustion side ($F^C_{Et,0}$) by means of variations in the ethanol molar fraction (dashed lines) and variations in the total flowrate (solid lines) for two particular temperatures of Fig. 6.

Fig. 6a the hydrogen yield shows a continuous increase up to values of 4 or higher. Conversely, when the fuel molar fraction is kept constant at $y^C_{Et,0} = 0.02$ and F^C_0 is augmented, the hydrogen yield hardly exceeds the value of 2 and the curve of η_{H_2} shows a maximum. In fact, increasing the total flowrate has two main consequences: the heat capacity of the fuel stream increases and the residence time on the combustion side diminishes. To the right of the maximum in the η_{H_2} curve, the oxidation reactions ($r4$) and ($r5$) take place close to the reactor outlet and the reforming reactions occurs in a shorter reactor length, resulting in a poorer hydrogen production. If further increases in the flowrate are selected, the combustion reactions are shifted outside the reactor and hence the maximum temperature and hydrogen yield drop significantly (see the detail in the lower right corner of Fig. 8).

4. Conclusions

From the previous results, the following conclusions can arise:

- The appropriate preheating of both process streams, together with adequate values of flowrate and ethanol molar fraction in the feed of the combustion side, are the keys to reach high production rates. If the operating conditions are correctly selected, the reactor will be ignited close to the entrance and high temperatures along the reactor length will take place, leading to low methane slips and high hydrogen yields.
- For fixed values of flowrate and composition of the feed streams, hydrogen yields relatively high were obtained ($2.6 < \eta_{H_2} < 3.4$) within a feasible range of temperatures for the Pd catalyst ($700 < T_{MAX} < 770$ °C). These maximum temperatures could still be reduced by means of an optimal selection of the air flowrate and ethanol molar fraction on the fuel side.
- Since ethanol combustion and ethanol steam reforming take place at very different reaction rates, designing a reformer for an efficient reaction coupling is a big challenge. The strongly exothermic ethanol combustion takes place in a narrow zone of the reactor, leading to a fast heat release. Thus, most of the catalyst on the fuel side is unemployed. This combustion heat cannot be consumed by the endothermic reactions at the same rate, because the steam reforming of ethanol is a slower process. Therefore, significant hot spots and strong temperature gradients can occur inside the reformer, with the consequent damage of the catalyst and/or the reactor materials. Further studies to explore alternatives of lateral feed of ethanol on the combustion side should be carried out, aiming to a smoother distribution of the heat generation along the reactor length.

Acknowledgments

Support of this work through Universidad Nacional del Sur (UNS) and Consejo Nacional de Investigaciones Científicas y Tecnológicas (CONICET) is gratefully acknowledged.

References

[1] S.E. Hosseini, M.A. Wahid, Hydrogen production from renewable sustainable energy resources: Promising green energy carrier for clean development, Renew. Rev. 57 (2016) 850–866.
[2] A. Bshish, Z. Yaakob, B. Narayanan, R. Ramakrishnan, A. Ebshish, Steam-reforming of ethanol for hydrogen production, Chem. Pap. 65 (2011) 251–266.
[3] I. Rossetti, M. Compagnoni, M. Torli, Process simulation and optimisation of H_2 production from ethanol steam reforming and its use in fuel cells. 1. Thermodynamic and kinetic analysis, Chem. Eng. J. 281 (2015) 1024–1035.
[4] I. Dancini-Pontes, M. DeSouza, F. AlvesSilva, M. HeloisaNeves, O. Scaliante, C. GoncalvesAlonso, G.S. Bianchi, A. MedinaNeto, G.M. Pereira, N.R. CamargoFernandes-Machado, Influence of the CeO_2 and Nb_2O_5 supports and

the inert gas in ethanol steam reforming for H_2 production, Chem. Eng. J. 273 (2015) 66–74.
[5] W. Ehrfeld, V. Hessel, H. Löwe, Microreactors, 1st ed., WILEY-VCH Verlag GmbH, Germany, 2000.
[6] I. Uriz, G. Arzamendi, E. López, J. Llorca, L.M. Gandía, Computational fluid dynamics simulation of ethanol steam reforming in catalytic wall microchannels, Chem. Eng. J. 167 (2011) 603–609.
[7] O. Görke, P. Pfeifer, K. Schubert, Kinetic study of ethanol reforming in a microreactor, Appl. Catal. A 360 (2009) 232–241.
[8] A.M. Anzola, Y.M. Bruschi, E. López, N.S. Schbib, M.N. Pedernera, D.O. Borio, Heat supply and hydrogen yield in an ethanol microreformer, Ind. Eng. Chem. Res. 50 (2011) 2698–2705.
[9] Y.M. Bruschi, E. López, N.S. Schbib, M.N. Pedernera, D.O. Borio, Theoretical study of the ethanol steam reforming in a parallel channel reactor, Int. J. Hydrogen Energy 37 (2012) 14887–14894.
[10] S.F. Weng, Y.H. Wang, C.S. Lee, Autothermal steam reforming of ethanol over $La_2Ce_{2-x}Ru_xO_7$ (x = 0–0.35) catalyst for hydrogen production, Appl. Catal. B 134–135 (2013) 359–366.
[11] C. Graschinsky, P. Giunta, N. Amadeo, M. Laborde, Thermodynamic analysis of hydrogen production by autothermal reforming of ethanol, Int. J. Hydrogen Energy 37 (2012) 10118–10124.
[12] R. Baruah, M. Dixit, P. Basarkar, D. Parikh, A. Bhargav, Advances in ethanol autothermal reforming, Renew. Sustain. Energy Rev. 51 (2015) 1345–1353.
[13] T. Hou, S. Zhang, T. Xu, W. Cai, Hydrogen production from oxidative steam reforming of ethanol over Ir/CeO_2 catalysts in a micro-channel reactor, Chem. Eng. J. 255 (2014) 149–155.
[14] A. Casanovas, M. Saint-Gerons, F. Griffon, J. Llorca, Autothermal generation of hydrogen from ethanol in a microreactor, Int. J. Hydrogen Energy 33 (2008) 1827–1833.
[15] M.R. Rahimpour, M.R. Dehnavi, F. Allahgholipour, D. Iranshashi, S.M. Jokar, Assessment and comparison of different catalytic coupling exothermic and endothermic reactions: A review, Appl. Energy 99 (2012) 496–512.
[16] A. Bakhtyari, M. Mohammadi, M.R. Rahimpour, Simultaneous production of dimethyl ether (DME), methyl formate (MF) and hydrogen from methanol in an integrated thermally coupled membrane reactor, J. Nat. Gas Sci. Eng. 26 (2015) 595–607.
[17] J. Frauhammer, G. Eigenberger, L.V. Hippel, D. Arntz, A new reactor concept for endothermic high-temperature reactions, Chem. Eng. Sci. 54 (1999) 3661–3670.
[18] G. Kolios, J. Frauhammer, G. Eigenberger, D. Arntz, Efficient reactor concepts for coupling of endothermic and exothermic reactions, Chem. Eng. Sci. 57 (2002) 1505–1510.
[19] G. Kolios, A. Gritsch, A. Morillo, U. Tuttlies, J. Bernnat, F. Opferkuch, G. Eigenberger, Heat-integrated reactor concepts for catalytic reforming and automotive exhaust purification, Appl. Catal. B 70 (2007) 16–30.
[20] E. López, V. Gepert, A. Gritsch, U. Nieken, G. Eigenberger, Ethanol steam reforming thermally coupled with fuel combustion in a parallel plate reactor, Ind. Eng. Chem. Res. 51 (2012) 4143–4151.
[21] Y.M. Bruschi, Estudio de micro-reactores para la generación de gas de síntesis, Thesis, Bahía Blanca, Argentina (UNS), 2014.
[22] J.M. Smith, H.C. Van Ness, M.M. Abbott, Introduction to Chemical Engineering Thermodynamics, sixth ed., McGraw Hill, Mexico, 2001.
[23] V. Hessel, S. Hardt, H. Löwe, Chemical Micro Process Engineering. Fundamentals, Modelling and Reactions, Wiley-VCH, Weinheim, Germany, 2004.
[24] I. Uriz, G. Arzamendi, P.M. Diéguez, F.J. Echave, O. Sanz, M. Montes, L.M. Gandía, CFD analysis of the effects of the flow distribution and heat losses on the steam reforming of methanol in catalytic (Pd/ZnO) microreactors, Chem. Eng. J. 238 (2014) 37–44.
[25] B.E. Poling, J.M. Prausnitz, J.P. O'Connell, The Properties of Gases and Liquids, fifth ed., McGraw-Hill, México, 2001.
[26] A. Cybulski, A. Stankiewicz, R.K. Edvinsson Albers, J.A. Moulijn, Monolithic reactors for fine chemicals industries: a comparative analysis of a monolithic reactor and a mechanically agitated slurry reactor, Chem. Eng. Sci. 54 (1999) 2351–2358.
[27] V. Mas, M.L. Bergamini, G. Baronetti, N. Amadeo, M.A. Laborde, Kinetic study of ethanol steam reforming using a nickel based catalyst, Top. Catal. 51 (2008) 39–48.